AGU PUBLICATIONS

Geophysical Research Letters

RESEARCH LETTER
10.1002/2016GL070655

Key Points:
- Skill in predicting the time trend of sea ice edge in the southern Pacific using the Southern Oscillation Index is examined
- Winter ice edge trends in the Pacific sector are partly associated with wind patterns linked to trend of the Southern Oscillation Index
- Low-frequency ice edge trends, linked to the natural variability of Southern Oscillation, are superimposed on anthropogenic forcing

Supporting Information:
- Supporting Information S1

Correspondence to:
R. Kwok,
ron.kwok@jpl.nasa.gov

Citation:
Kwok, R., J. C. Comiso, T. Lee, and P. R. Holland (2016), Linked trends in the South Pacific sea ice edge and Southern Oscillation Index, *Geophys. Res. Lett.*, *43*, 10,295–10,302, doi:10.1002/2016GL070655.

Received 29 JUL 2016
Accepted 27 SEP 2016
Accepted article online 28 SEP 2016
Published online 9 OCT 2016

Linked trends in the South Pacific sea ice edge and Southern Oscillation Index

R. Kwok[1], J. C. Comiso[2], T. Lee[1], and P. R. Holland[3]

[1]Jet Propulsion Laboratory, California Institute of Technology, Pasadena, California, USA, [2]NASA/Goddard Space Flight Center, Greenbelt, Maryland, USA, [3]British Antarctic Survey, Cambridge, UK

Abstract Previous work have shown that sea ice variability in the South Pacific is associated with extratropical atmospheric anomalies linked to the Southern Oscillation (SO). Over a 32 year period (1982–2013), our study shows that the trend in Southern Oscillation Index (SOI) is also able to quantitatively explain the trends in sea ice edge, drift, and surface winds in this region. On average two thirds of the winter ice edge trend in this sector, linked to ice drift and surface winds, could be explained by the positive SOI trend, thus subjecting the ice edge to strong decadal SO variability. If this relationship holds, the negative SOI trend prior to the recent satellite era suggests that ice edge trends opposite to that of the recent record over a similar time scale. Significant low-frequency ice edge trends, linked to the natural variability of SO, are superimposed upon any trends expected of anthropogenic forcing.

1. Introduction

The increase in overall Antarctic sea ice extent over the satellite record is the sum of larger opposing trends in different sectors of the Southern Ocean [*Comiso and Nishio*, 2008; *Comiso et al*., 2011; *Holland*, 2014]. To date, there is no consensus on the causes, but a variety of mechanisms have been proposed: stratospheric ozone depletion [e.g., *Turner et al*., 2009], connections to variability of the Southern Oscillation and Southern Annular Mode [e.g., *Yuan and Martinson*, 2000; *Kwok and Comiso*, 2002b; *Stammerjohn et al*., 2008], increased precipitation [e.g., *Liu and Curry*, 2010], increased discharge of glacial meltwater [e.g., *Bintanja et al*., 2013], connections to Atlantic warming [*Li et al*., 2014], and weakened ocean heat flux [*Haumann et al*., 2014]. Results from recent studies [*Holland and Kwok*, 2012; *Zhang*, 2014] reveal large and statistically significant trends in Antarctic ice drift in most sectors that are associated with intensification of surface winds, suggesting that regional wind-driven changes may be the dominant drivers of ice extent around much of Antarctica. An understanding of the sources of the trends in local wind anomalies and how they are linked to the global climate system may enable us to address deficiencies in climate models, which have failed to reproduce the overall increase in Antarctic ice extent let alone the regional patterns in ice extent [e.g., *Mahlstein et al*., 2013; *Polvani and Smith*, 2013; *Turner et al*., 2015; *Zunz et al*., 2013; *Hobbs et al*., 2015]. One source of wind anomalies is the high-latitude atmospheric anomalies in the Pacific sector of the Southern Ocean linked to the Southern Oscillation (SO)—the focus of this note.

The Southern Oscillation (SO) refers to the seesaw in sea level pressure (SLP) anomalies between the Indian Ocean-Australian region and the southeastern tropical Pacific on seasonal to interannual time scales [*Philander and Rasmusson*, 1985]. The climate anomalies associated with the SO extend to high southern latitudes in winter and summer, affecting regional atmospheric circulation and thus the behavior of the Antarctic sea ice cover. The strongest correlation between the Southern Oscillation Index (SOI; a measure of the strength and phase of the SO) and Southern Hemisphere climate anomalies is found in the Pacific sector of the Southern Ocean, which includes the Amundsen, Bellingshausen, and Ross Seas [e.g., *Yuan and Martinson*, 2000; *Kwok and Comiso*, 2002a; *Yuan*, 2004; *Stammerjohn et al*., 2008; *Simpkins et al*., 2012]. Within this sector, poleward and equatorward wind anomalies are linked to quasi-stationary atmospheric pressure anomalies associated with the SO, centered several hundreds of kilometers north of the Antarctic coast, where positive (negative) phases of the SOI are generally associated with lower (higher) sea level pressure, cooler (warmer) surface air temperature, and cooler (warmer) sea surface temperature.

Studies over the last decade or so have established that surface wind anomalies in the Pacific sector, linked to the SO, contribute to the variability of Antarctic sea ice extent [*Yuan and Martinson*, 2000; *Kwok and Comiso*, 2002a; *Yuan*, 2004; *Stammerjohn et al*., 2008; *Yuan and Li*, 2008; *Simpkins et al*., 2012]. Here our motivation is to

examine in more detail and focus on the quantitative skill in the use of the Southern Oscillation Index (SOI)—its trend and variability—in diagnosing the time trend and variability of the winter sea ice edge, drift, and surface winds. If skill were demonstrated, then the SOI time series may be used as a proxy of sea ice behavior prior to the present 32 year record. To address this, we use a 32 year record (1982–2013) to examine the winter connections between ice edge location, ice drift, and the SOI time series. The SOI is the normalized difference between the standardized Tahiti sea level pressure (SLP) and the standardized Darwin SLP measurements, and El Niño episodes refer to large negative excursions of the SOI. Here we focus on the July–November period since the correlation between the SOI and ice edge and the quantitative skill of the SOI in predicting its trend are highest during this period (discussed later in section 3.2).

The next section describes the data set used. Section 3 outlines our analysis methodology, describes the linkage between the SOI and surface climate anomalies in the Pacific sector, and provides an analysis of the use of the SOI time trend to predict ice edge and surface climate anomalies. The last section summarizes our findings and the implications of the results.

2. Data Description

2.1. Sea Ice Edge and Drift

The locations of the time-varying ice edge used here are sampled at longitudinal increments of 1° (i.e., 360 increments are used to define the circumpolar ice edge). Ice edge is the latitudinal location where the ice concentration first exceeds 15% in the transition from open ocean to the consolidated ice cover. Gridded maps of ice concentration (1982–2013) are derived from the Scanning Multi-channel Microwave Radiometer (SMMR) and Special Sensor Microwave Imager (SSM/I) data using the bootstrap algorithm [*Comiso and Nishio*, 2008].

Monthly ice drifts used here are averages of 2 day motion fields from satellite retrievals [*Kwok et al*., 1998]. The gridded fields of sea ice motion $\rightarrow u$ (100 km spacing)—on a polar stereographic projection—used here are constructed by blending ice motion derived from two satellite radiometer channels (37 GHz and 85 GHz), viz.,

$$\widehat{\vec{u}}(x,y) = \sum_i \alpha_i \vec{u}_i^{\ 85\ \ \mathrm{GHz}} + \sum_j \beta_j \vec{u}_j^{\ 37\ \ \mathrm{GHz}},$$

where α and β are the weighting coefficients determined by an optimal interpolation scheme [*Kwok et al*., 2013]; the indices i and j are the available observations from each radiometer channel. A spatial correlation length scale of 300 km is used to create the interpolated field. This length scale is selected as an intermediate length scale based on the density of satellite observations but short enough that the expressions of coastal effects are not noticeably degraded. A consistent and updated time series of passive microwave brightness temperature and ice concentration fields were used to produce the satellite ice drifts. Uncertainties in the 2 day drift estimates from the SMMR (1982–1987) [*Gloersen*, 2006] and SSM/I (1988–present) [*Maslanik and Stroeve*, 2004] data sets are between 3 and 6 km (depending on spatial resolution of the passive microwave channel) for individual displacement vectors. Ice motion fields from multiple channels on the same instrument (e.g., 37 GHz and 85 GHz on SSM/I) are used when they are available. Together, the length of the ice drift record provided by the combination of sensors spans more than three decades. Our records start in 1982 to avoid gaps in the earlier brightness temperature fields. Based on the number of observation and expected uncertainties in the passive microwave ice motion estimates, the procedure above provides an analysis of the error of each motion estimate. An expected average uncertainty of 3–4 km/d in the individual interpolated estimates is typical, although the uncertainty varies with the density of measurements available within the neighborhood of each estimate.

2.2. Other Data Sets

Also used are sea level pressure and wind fields from the ERA-Interim atmospheric reanalysis project (http://data-portal.ecmwf.int/data/d/interim_daily/) and Southern Oscillation Index (SOI) from National Climatic Data Center (NCDC) (www.ncdc.noaa.gov/teleconnections/enso/indicators/soi/) for the same period.

3. Data Analysis

In this section, we describe the use of ice edge in our analysis; the correlations between time-varying ice edge and SOI; the linkage between SOI and sea ice and surface climate anomalies; and finally, the concurrent time trends in the SOI, ice edge, and surface climate anomalies.

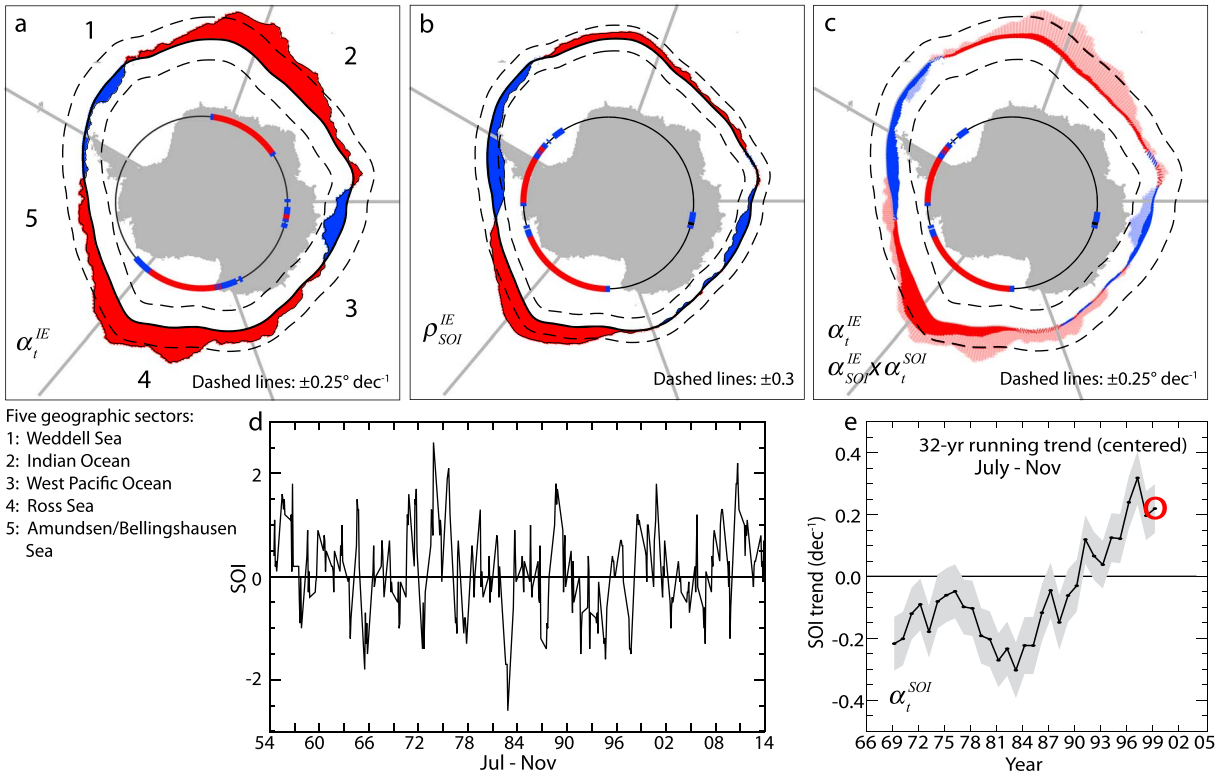

Figure 1. Winter (July–November) trends in sea ice edge (IE) and Southern Oscillation Index (SOI). (a) Trends in IE (in degrees of latitude per decade) relative to the mean July–November IE (red positive/blue negative) for 1982–2013. (b) Correlations between detrended IE and detrended SOI (red positive/blue negative). (c) Trends in IE (same as in Figure 1a but in lighter shade) and calculated time trend associated with the SOI (i.e., product of SOI trend and coefficients from regression of IE against SOI (1982–2013)). (d) Monthly SOI between 1954 and 2013. (e) Running 32 year SOI trends (centered) between 1954 and 2014; the gray shading shows the ±1 standard deviation of running 32 year trend, and the red circle shows the recent 32 year trend (1982–2013) addressed here. Also shown are the five geographic sectors typically used for calculation of trends in ice extent. The color of interior circles shows the confidence level in the trend (blue: >95%, red: >99%, and black: ≤95%).

3.1. Ice Edge Location

Instead of utilizing trends in total ice extent in five predefined sectors of the Southern Ocean [*Comiso and Nishio*, 2008], typically used in published ice extent analyses, Figure 1a shows the July–November trends in ice edge (IE) location, $\alpha_t^{IE}(\lambda)$, encircling the pole in the 32 year record. (Henceforth, α_x^y denotes a linear regression coefficient, α, which relates a dependent variable (y) and an independent variable (x)). With this spatial depiction (Figure 1a), the variability of circumpolar trends in ice edge, at 1° increments of longitude (λ), is better resolved. The trends are plotted relative to the mean July–November ice edge locations to highlight the distance of the winter ice edge from the continent and for easier identification of corresponding ice edge and regional climate anomalies away from coastal Antarctica (Figures 2 and 3).

It can be seen in the circumpolar wave number 2 pattern that the predominantly positive trends in ice edge (in red) contributed to the overall equatorward expansion of the winter ice edge around the continent. There are two distinct lobes with positive ice edge trends: one that spans the Ross, Amundsen, and Bellingshausen Seas between roughly 150°E and 90°W (clockwise), while the other straddles part of the Atlantic and Indian Oceans, between ~30°W and 60°E. These circumpolar trends also suggest that the five geographically predefined sectors used in earlier studies (delineated by the radial lines in Figure 1) do not necessarily coincide with regions showing distinct sea ice trends. This was also noted by others [e.g., *Raphael and Hobbs*, 2014], who have identified distinct regions of sea ice trends and variability around the Antarctic continent.

3.2. Correlations Between Time-Varying Ice Edge and SOI

Associations between the SOI and circumpolar ice edge locations are most evident in the correlations between the time records. The results (Figure 1b) show a wave number 2 pattern that is substantially similar

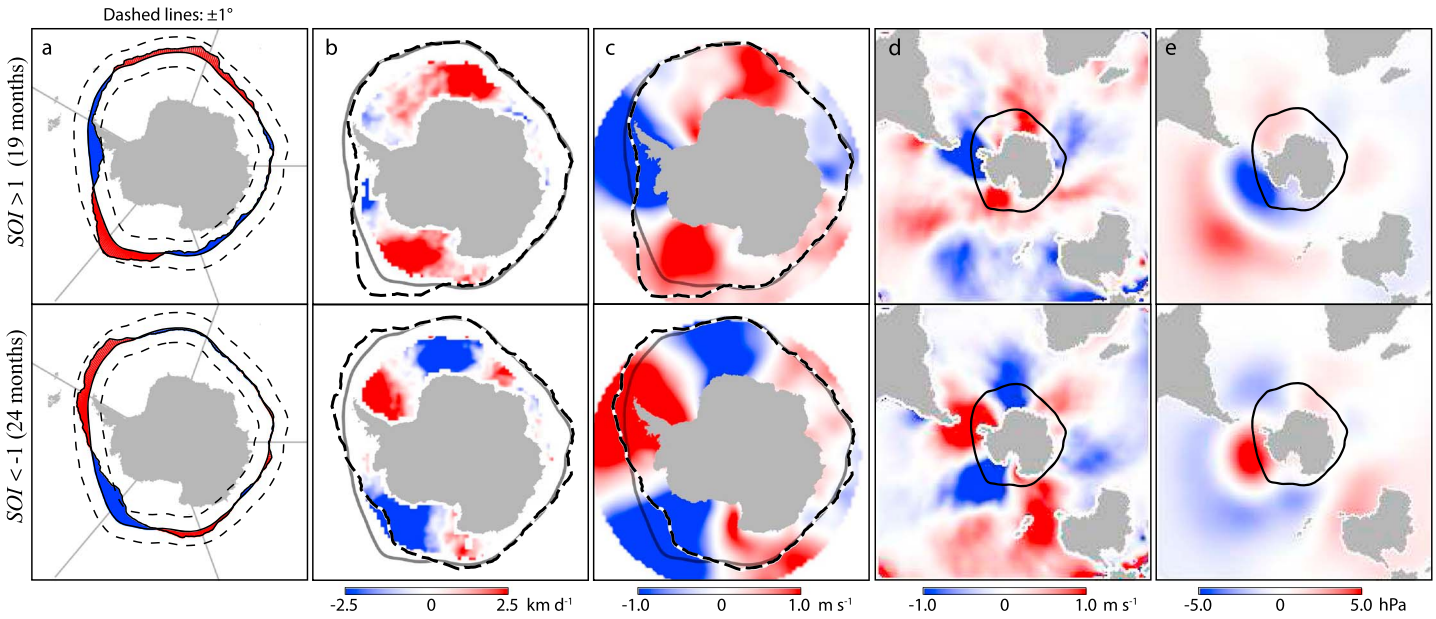

Figure 2. Composites of ice and surface climate anomalies in positive/negative phases of SOI. (a) Ice edge, (b) meridional ice motion, (c) meridional winds (in sea ice zone), (d) meridional winds (hemispheric scale), and (e) sea level pressure during the (top) positive (SOI > 1) and (bottom) negative phases (SOI < -1) of SOI (1982–2013). Ice edge anomalies are plotted on the mean July–November IE for 1982–2013. The dashed contours in Figures 2b and 2c are the ice edge anomalies from Figure 2a. The light gray contours in Figures 2b and 2c and black contours in Figure 2e are the mean July–November ice edge. The loading (number of month) of each composite pattern is also shown.

to that of the ice edge trends in Figure 1a (i.e., the locations of the positive and negative lobes). Both records were detrended prior to the calculations to remove correlations due to corresponding trends. Statistically significant correlations (>95% confidence level) found in the Pacific sector (hereinafter defined to be between ~180°E and 60°W) show the expected regional connection of the ice edge to the extratropical anomalies of SO (Figures 1b and 1c). At the maximum in the circumpolar trend (~160°W longitude), the SOI explains ~28% of the variance in the ice edge. As mentioned earlier, we use only the July–November period because of the significance and spatial coherence in the correlation between the SOI and IE anomalies and because the quantitative skill of the SOI in predicting the ice edge trend is highest between July and November (Figure 1b; also see Figure S1). *Jin and Kirtman* [2009] also noted that July–November are the months when the SO teleconnection is strongest. Even though Southern Ocean sea ice trends may be more significant in summer and fall [*Hobbs et al.*, 2015], and that fall trends may be driven by anomalies in the previous retreat season [*Stammerjohn et al.*, 2012; *Holland*, 2014], the focus here is on the skill of the SOI during the winter in the available ice edge and surface climate records.

To assess the quantitative skill of the SOI in predicting the time trend of the ice edge, we regressed the ice edge against the SOI; the regression coefficient $\left(\alpha^{\mathrm{IE}}_{\mathrm{SOI}}(\lambda)\right)$ relates the changes in ice edge location corresponding to a unit change in the standardized index. The product of the regression coefficient $\left(\alpha^{\mathrm{IE}}_{\mathrm{SOI}}(\lambda)\right)$ and the time trend of the SOI $\left(\alpha^{\mathrm{SOI}}_{t}\right)$ then yield estimates of the time trend in ice edge (viz., $\tilde{\alpha}^{\mathrm{IE}}_{t}(\lambda) = \alpha^{\mathrm{IE}}_{\mathrm{SOI}}(\lambda) \times \alpha^{\mathrm{SOI}}_{t}$, where "~" denotes the estimated time trend) in Figure 1c. Over the record, the time trend in the SOI as plotted in Figure 1e points to a positive time trend of $0.2 \pm 0.06\ \mathrm{dec}^{-1}$ or an overall increase of >0.6 in the standardized index over the 32 year record. We note here that the SOI time trend (Figure 1e) does not depend on longitude.

The estimated $\left(\tilde{\alpha}^{\mathrm{IE}}_{t}(\lambda)\right)$ and observed $\left(\alpha^{\mathrm{IE}}_{t}(\lambda)\right)$ time trends in ice edge are compared in Figure 1c. It can be seen that the magnitudes of the estimated and observed trends are best matched within the Pacific sector (again, between ~180°E and 60°W). Where the significance level is >95% (indicated by the red and blue colors in interior circles), the estimated trends explain on average more than 65% of the observed trends (i.e., by averaging the ratios of the two trends where the ratios are <1.0). Away from the Pacific sector, the estimated ice edge trends predicted by the SOI trend are smaller and have reduced significance.

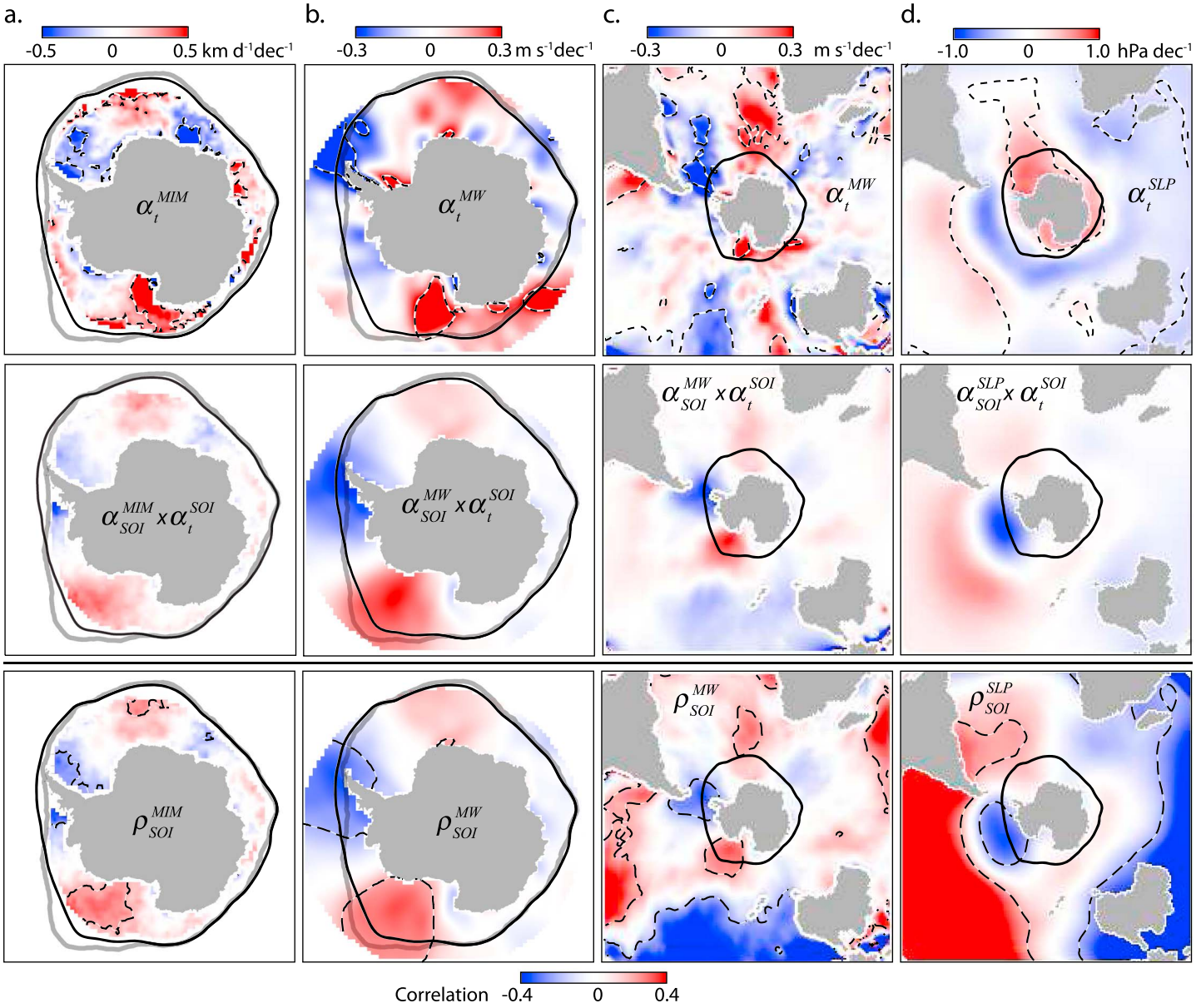

Figure 3. (top) Comparison of observed time trends with (middle) calculated trends associated with the SOI for the 32 year record (1982–2013). (a) Meridional ice motion, (b) meridional winds (in sea ice zone), (c) meridional winds (hemispheric scale), and (d) sea level pressure. The middle plots show the products between SOI regression maps and the SOI time trend, and the bottom plots show the detrended correlations with SOI. The gray contours in Figures 3a and 3b are the calculated ice edge trends from Figure 1c. The black contours are the mean July–November IE. Trends within dashed contours are significant at >95% level.

3.3. SOI, Ice, and Surface Climate Anomalies

To visualize the role of SO-induced climate anomalies in the Pacific sector, one approach is to examine the relationship between the monthly ice edge/surface climate anomalies and extremes in the SOI (in the 32 year record) by constructing composite maps that show the spatial character of these anomalies during positive (SOI^+: $SOI > 1.0$) and negative (SOI^-: $SOI < -1.0$) extremes of the SOI (1982–2013) [following *Kwok and Comiso*, 2002a]. The anomalies are ice edge, meridional ice motion, meridional wind, and sea level pressure (SLP). While the composites by *Kwok and Comiso* [2002a, Figure 7] were of a shorter 17 year data set, the anomalies show similar spatial patterns.

The SOI^+ and SOI^- composite maps in (Figure 2) show anomalies that are organized in distinct spatial patterns with nearly opposing polarities at the two extremes of SOI (also reported in other studies [e.g., *Kwok and*

Comiso, 2002a; *Yuan*, 2004; *Stammerjohn et al*., 2008; *Yuan and Li*, 2008; *Simpkins et al*., 2012]). In the Pacific sector, the positive ice edge anomalies in the eastern Ross/Amundsen Seas and the negative ice edge anomalies in the Bellingshausen Sea in the SOI^+ composite (Figure 2a) resemble the pattern in the observed trends (Figure 1a). Further, the regions with positive/negative anomalies in ice edge coincide with the positive/negative anomalies in meridional ice motion and winds. The polarities of the meridional ice motion and wind anomalies are expected to be positively correlated because ice drift is largely wind driven [*Thorndike and Colony*, 1982]; this lends credence to the substantial influence of wind-driven ice drift on ice edge anomalies discussed by *Holland and Kwok* [2012]. While these composite maps also suggest potential asymmetry in the mean response of the ice edge during SOI^+ and SOI^- phases, the loading of two spatial patterns (i.e., the number of months in each composite: 19 and 24) seems insufficient and unbalanced to address potential asymmetries in the response.

On a near-hemispheric scale, the large-scale meridional wind anomalies of opposing polarities extend beyond the sea ice zone of the Southern Ocean into the Pacific, Atlantic, and Indian Oceans (Figure 2d). These wind anomalies are associated with the large-scale pattern of SLP anomalies centered north of Antarctic coast at ~60°S and ~130°W. During SOI^+, the low-pressure anomaly leads to anomalous poleward winds in the Bellingshausen Sea and equatorward winds in the Amundsen and Ross Seas. The opposite behavior is seen during SOI^-. Also evident is the characteristic out-of-phase behavior in SLP between tropical and polar latitudes in the Pacific sector (Figure 2e). In each of recent La Niña/El Niño episodes (i.e., extreme positive/negative phases of the SOI) over the last several decades, significant and correlated changes of the sea ice in the Bellingshausen and Amundsen Seas were reported [e.g., *Kwok and Comiso*, 2002a], showing unique associations of the Pacific sector of the Antarctic with the SO. This suggests that trends in the SOI may be useful in understanding not only variability but also trends in ice edge behavior in this sector.

3.4. Predicted Time Trends

While the composite maps (in Figure 2) show the opposite behavior of the four surface parameters (ice edge, meridional ice motion, meridional winds, and SLP) in the positive and negative extremes of SOI, they do not show how their trends are related to trends in the SOI. To do this, we first examine maps of the time trends of these parameters $\left(\alpha_t^{\mathrm{MM}}(\lambda),\ \alpha_t^{\mathrm{MW}}(\lambda),\ \text{and}\ \alpha_t^{\mathrm{SLP}}(\lambda)\right)$ (Figure 3a, top). Broadly, over the 32 year record, the polarities in the time trends are the same as the polarities of the anomalies in the SOI^+ composites (Figure 2a). Spatially, the positive/negative anomalies coincide with positive/negative trends. These correspondences suggest a positive tendency in the SOI time trend. Away from the Pacific sector, however, we do not observe—and it is not expected—that the time-trend patterns share corresponding patterns with the patterns in the SOI phases, as there are contributions by other physical processes to the overall time trend (e.g., those associated with variability in the Atlantic and Indian Ocean sectors).

Also of interest is the covariance between the surface climate parameters (ice, wind, and SLP) and SOI (ρ_{SOI}^x, where x is the surface parameter). The correlation maps (Figure 3, bottom) of the detrended parameters show the regions where these parameters are significantly correlated to the SOI. As expected, correlations are strongest in the Pacific sector, and areas with positive/negative correlations in wind/ice motion correspond to regions with positive/negative SOI-related trends in ice edge. This reinforces the connection between the regional ice edge anomalies with the meridional ice motion that are forced by meridional winds associated with the trends in SLP anomalies, which are linked to the SO off the coast of Antarctica.

Lastly, the skill of the SOI can be assessed and quantified by forming the product between the time trend of the SOI $\left(\alpha_t^{\mathrm{SOI}}\right)$ and the regression map, in this case, for each surface parameter x (i.e., $\alpha_{\mathrm{SOI}}^x(\varphi,\lambda)$, where φ is the latitude and λ is the longitude). As above, the regression map quantifies changes of the given parameter corresponding to a unit change in the SOI index and the product (i.e., $\widetilde{\alpha}_t^x(\varphi,\lambda) = \alpha_{\mathrm{SOI}}^x(\varphi,\lambda)\times\alpha_t^{\mathrm{SOI}}$) provides linear estimates of the estimated trend. As can be seen in Figure 3 (middle), the estimated trends are comparable to the observed time trends ($\alpha_t^x(\varphi,\lambda)$; Figure 3, top). Indeed, the patterns in the predicted and observed trend map in Figure 3 show that within the Pacific sector, there are remarkable spatial correspondences between the observed trends and those predicted using the trend in the SOI. Again, the trends associated with the SOI are smaller and less significant away from the Pacific sector and from the influence of the Southern Oscillation.

4. Conclusions

In this note, the quantitative skill of the Southern Oscillation Index (SOI) in predicting the time trend and variability of the sea ice edge, drift, and surface winds (1982–2013) is examined. It is recognized that the trends of the circumpolar Antarctic ice edge are complex and that these trends may be expressions of a variety of physical mechanisms—some of which are listed in the Introduction. Here our analysis is focused on only the surface climate anomalies in the Pacific sector (between ~180°E and 60°W) that are connected to variability of the SO during winter. The 32 year trend (1982–2013) of winter ice edge, ice drift, and surface winds in the Pacific sector of the Antarctic—negative in the Bellingshausen Sea and positive in the Amundsen and Ross Seas—are shown to be linked to a positive trend in the SOI. Regression analysis shows that on average two thirds of the observed winter (July–November) ice edge trend in this sector can be explained by the positive SOI trend. This result indicates uniquely that the location of ice edge and regional climate anomalies in the Pacific sector of the Southern Ocean are strongly correlated to decadal-scale SO variability.

In the Pacific sector, our analysis suggests that the SO contributes not only to the wind anomalies that drive the variability of the local ice drift and ice edge but also to their time trends. With the demonstrated skill of the SOI for predicting the ice edge location in the Pacific sector, variability in the 32 year running trends of the SOI can be used as a proxy for examining past behavior in the regional ice edge and to assess whether ice edge trends have varied over the longer SOI record. Indeed, the time series of 32 year running trend since 1954 (Figure 1e) exhibits low-frequency decadal-scale variability in the SOI with large negative excursions in the 32 year trends (and thus ice edge trends) between the beginning of the record and the early 1990s, before turning positive in the early 1990s. This reversal in the sign of the trends is consistent with reanalysis of Southern Ocean climate variations since the 1950s [*Fan et al*., 2014] and coastal ice core records in the Ross, Amundsen, and Bellingshausen Seas [*Sinclair et al*., 2014; *Abram et al*., 2010; *Thomas and Abram*, 2016]. Consequently, trends in regional ice extent in the Pacific sector are subject to decadal-scale variability of the SO—the strongest source of natural variability in the Earth's climate system [*Philander*, 1990], and the ability to capture the trends associated with the natural variability as caused by SO would be desirable but a challenge for the current generation of climate models [*Mahlstein et al*., 2013; *Polvani and Smith*, 2013; *Turner et al*., 2015; *Zunz et al*., 2013].

Acknowledgments

R.K. and T.L. carried out this work at the Jet Propulsion Laboratory, California Institute of Technology, under a contract with the National Aeronautics and Space Administration. The optimally interpolated monthly ice drift and ice edge data sets are available at http://rkwok.jpl.nasa.gov/icemotion. Sea level pressure and wind fields are from the ERA-Interim atmospheric reanalysis (http://data-portal.ecmwf.int/data/d/interim_daily/) and the Southern Oscillation Index from NCDC (www.ncdc.noaa.gov/teleconnections/enso/indicators/soi/).

References

Abram, N. J., E. R. Thomas, J. R. McConnell, R. Mulvaney, T. J. Bracegirdle, L. C. Sime, and A. J. Aristarain (2010), Ice core evidence for a 20th century decline of sea ice in the Bellingshausen Sea, Antarctica, *J. Geophys. Res.*, *115*, D23101, doi:10.1029/2010JD014644.

Bintanja, R., G. J. van Oldenborgh, S. S. Drijfhout, B. Wouters, and C. A. Katsman (2013), Important role for ocean warming and increased ice-shelf melt in Antarctic sea-ice expansion, *Nat. Geosci.*, *6*(5), 376–379, doi:10.1038/ngeo1767.

Comiso, J. C., and F. Nishio (2008), Trends in the sea ice cover using enhanced and compatible AMSR-E, SSM/I, and SMMR data, *J. Geophys. Res.*, *113*, C02S07, doi:10.1029/2007JC004257.

Comiso, J. C., R. Kwok, S. Martin, and A. L. Gordon (2011), Variability and trends in sea ice extent and ice production in the Ross Sea, *J. Geophys. Res.*, *116*, C04021, doi:10.1029/2010JC006391.

Fan, T. T., C. Deser, and D. P. Schneider (2014), Recent Antarctic sea ice trends in the context of Southern Ocean surface climate variations since 1950, *Geophys. Res. Lett.*, *41*, 2419–2426, doi:10.1002/2014GL059239.

Gloersen, P. (2006), Nimbus-7 SMMR Polar Gridded Radiances and Sea Ice Concentrations, version 1, NASA Natl. Snow and Ice Data Cent. Distrib. Act. Arch. Cent., Boulder, Colo., doi:10.5067/QOZIVYV3V9JP.

Haumann, F. A., D. Notz, and H. Schmidt (2014), Anthropogenic influence on recent circulation-driven Antarctic sea ice changes, *Geophys. Res. Lett.*, *41*, 8429–8437, doi:10.1002/2014GL061659.

Hobbs, W. R., N. L. Bindoff, and M. N. Raphael (2015), New perspectives on observed and simulated Antarctic Sea ice extent trends using optimal fingerprinting techniques, *J. Clim.*, *28*(4), 1543–1560, doi:10.1175/JCLI-D-14-00367.1.

Holland, P. R. (2014), The seasonality of Antarctic sea ice trends, *Geophys. Res. Lett.*, *41*, 4230–4237, doi:10.1002/2014GL060172.

Holland, P. R., and R. Kwok (2012), Wind-driven trends in Antarctic sea-ice drift, *Nat. Geosci.*, *5*(12), 872–875, doi:10.1038/ngeo1627.

Jin, D., and B. P. Kirtman (2009), Why the Southern Hemisphere ENSO responses lead ENSO, *J. Geophys. Res.*, *114*, D23101, doi:10.1029/2009JD012657.

Kwok, R., and J. C. Comiso (2002a), Southern Ocean climate and sea ice anomalies associated with the Southern Oscillation, *J. Clim.*, *15*(5), 487–501.

Kwok, R., and J. C. Comiso (2002b), Spatial patterns of variability in Antarctic surface temperature: Connections to the Southern Hemisphere Annular Mode and the Southern Oscillation, *Geophys. Res. Lett.*, *29*(14), 1705, doi:10.1029/2002GL015415.

Kwok, R., A. Schweiger, D. A. Rothrock, S. Pang, and C. Kottmeier (1998), Sea ice motion from satellite passive microwave imagery assessed with ERS SAR and buoy motions, *J. Geophys. Res.*, *103*, 8191–8214, doi:10.1029/97JC03334.

Kwok, R., G. Spreen, and S. Pang (2013), Arctic sea ice circulation and drift speed: Decadal trends and ocean currents, *J. Geophys. Res. Oceans*, *118*, 2408–2425, doi:10.1002/jgrc.20191.

Li, X., D. M. Holland, E. P. Gerber, and C. Yoo (2014), Impacts of the North and tropical Atlantic Ocean on the Antarctic Peninsula and sea ice, *Nature*, *505*(7484), 538–542, doi:10.1038/nature12945.

Liu, J. P., and J. A. Curry (2010), Accelerated warming of the Southern Ocean and its impacts on the hydrological cycle and sea ice, *Proc. Natl. Acad. Sci. U.S.A.*, *107*(34), 14,987–14,992, doi:10.1073/pnas.1003336107.

Mahlstein, I., P. R. Gent, and S. Solomon (2013), Historical Antarctic mean sea ice area, sea ice trends, and winds in CMIP5 simulations, *J. Geophys. Res. Atmos.*, *118*, 5105–5110, doi:10.1002/jgrd.50443.
Maslanik, J., and J. Stroeve (2004), DMSP SSM/I-SSMIS daily polar gridded brightness temperatures, version 4, (updated 2012), NASA DAAC at the Natl. Snow and Ice Data Cent., Boulder, Colo.
Philander, S. G. (1990), *El Niño, La Niña, and the Southern Oscillation*, Academic, San Diego, Calif.
Philander, S. G., and E. M. Rasmusson (1985), The Southern Oscillation and El Niño, *Adv. Geophys.*, *28*, 197–215.
Polvani, L. M., and K. L. Smith (2013), Can natural variability explain observed Antarctic sea ice trends? New modeling evidence from CMIP5, *Geophys. Res. Lett.*, *40*, 3195–3199, doi:10.1002/grl.50578.
Raphael, M. N., and W. Hobbs (2014), The influence of the large-scale atmospheric circulation on Antarctic sea ice during ice advance and retreat seasons, *Geophys. Res. Lett.*, *41*, 5037–5045, doi:10.1002/2014GL060365.
Simpkins, G. R., L. M. Ciasto, D. W. J. Thompson, and M. H. England (2012), Seasonal relationships between large-scale climate variability and Antarctic Sea ice concentration, *J. Clim.*, *25*(16), 5451–5469, doi:10.1175/Jcli-D-11-00367.1.
Sinclair, K. E., N. A. N. Bertler, M. M. Bowen, and K. R. Arrigo (2014), Twentieth century sea-ice trends in the Ross Sea from a high-resolution, coastal ice-core record, *Geophys. Res. Lett.*, *41*, 3510–3516, doi:10.1002/2014GL059821.
Stammerjohn, S. E., D. G. Martinson, R. C. Smith, X. Yuan, and D. Rind (2008), Trends in Antarctic annual sea ice retreat and advance and their relation to El Niño–Southern Oscillation and Southern Annular Mode variability, *J. Geophys. Res.*, *113*, C03S90, doi:10.1029/2007JC004269.
Stammerjohn, S. E., R. Massom, D. Rind, and D. Martinson (2012), Regions of rapid sea ice change: An inter-hemispheric seasonal comparison, *Geophys. Res. Lett.*, *39*, L06501, doi:10.1029/2012GL050874.
Thomas, E. R., and N. J. Abram (2016), Ice core reconstruction of sea ice change in the Amundsen-Ross Seas since 1702 AD, *Geophys. Res. Lett.*, *43*, 5309–5317, doi:10.1002/2016GL068130.
Thorndike, A. S., and R. Colony (1982), Sea ice motion in response to geostrophic winds, *J. Geophys. Res.*, *87*, 5845–5852, doi:10.1029/JC087iC08p05845.
Turner, J., J. C. Comiso, G. J. Marshall, T. A. Lachlan-Cope, T. Bracegirdle, T. Maksym, M. P. Meredith, Z. M. Wang, and A. Orr (2009), Non-annular atmospheric circulation change induced by stratospheric ozone depletion and its role in the recent increase of Antarctic sea ice extent, *Geophys. Res. Lett.*, *36*, L08502, doi:10.1029/2009GL037524.
Turner, J., J. S. Hosking, T. J. Bracegirdle, G. J. Marshall, and T. Phillips (2015), Recent changes in Antarctic Sea ice, *Philos. Trans. A Math. Phys. Eng. Sci.*, *373*(2045), 20140163, doi:10.1098/rsta.2014.0163.
Yuan, X. (2004), ENSO-related impacts on Antarctic sea ice: A synthesis of phenomenon and mechanisms, *Antarct. Sci.*, *16*(4), 415–425, doi:10.1017/s0954102004002238.
Yuan, X., and C. Li (2008), Climate modes in southern high latitudes and their impacts on Antarctic sea ice, *J. Geophys. Res.*, *113*, C06S91, doi:10.1029/2006JC004067.
Yuan, X., and D. G. Martinson (2000), Antarctic sea ice extent variability and its global connectivity, *J. Clim.*, *13*(10), 1697–1717, doi:10.1175/1520-0442(2000)013<1697:Asieva>2.0.Co;2.
Zhang, J. (2014), Modeling the impact of wind intensification on Antarctic Sea ice volume, *J. Clim.*, *27*(1), 202–214, doi:10.1175/jcli-d-12-00139.1.
Zunz, V., H. Goosse, and F. Massonnet (2013), How does internal variability influence the ability of CMIP5 models to reproduce the recent trend in Southern Ocean sea ice extent?, *Cryosphere*, *7*(2), 451–468, doi:10.5194/tc-7-451-2013.